

## A theoretical analysis of the nonadiabatic photodissociation of HF and DF molecules: fine-structure distributions of the $F(^2P_J)$ product

Yuan-Jun Li<sup>a,b</sup>, Pei-Yu Zhang<sup>a,b</sup>, and Ke-Li Han<sup>a,\*</sup>

<sup>a</sup> State Key Laboratory of Molecular Reaction Dynamics, Dalian Institute of Chemical Physics, Chinese Academy of Sciences, Dalian 116023, China

<sup>b</sup> Graduate School of the Chinese Academy of Sciences, Beijing 100049, China

Received 25 January 2010; Accepted (in revised version) 8 February 2010;

Available online 15 February 2010

---

**Abstract.** A theoretical analysis is presented for the nonadiabatic photodissociation process of hydrogen fluoride and its deuterated species. Four electronic states  $X^1\Sigma^+$ ,  $a^3\Pi$ ,  $A^1\Pi$ , and  $^3\Sigma^+$  are involved in the studies. Based on the accurate *ab initio* calculations of the potential energy curves, transition dipole moment and spin-orbit couplings among the accessible states, the time dependent quantum wave packet approach with the split-operator scheme is employed to investigate the dissociative dynamics. The dissociative process is analyzed via the evolution of the wave packets. The total cross sections, partial cross sections and branching fractions for both HF and DF initially excited from the vibrational levels  $v=0-3$  of the ground state are evaluated. The calculations are compared with the previous investigations and the present prediction for a broad range of the incident photon energies.

PACS: 33.80.Gj

**Key words:** photodissociation, nonadiabatic interactions, quantum dynamics, time dependent wave packet, split-operator, cross section, branching fraction

---

## 1 Introduction

Photodissociation involving multiple dissociative pathways via the nonadiabatic interactions is one of the most interesting phenomena in the interactions between photons and molecules (or radicals) [1–8]. The closed-shell hydrogen halide (HX, X=F, Cl, Br, I) and its deuterated counterpart, provides the typical and simple model to investigate the dynamics of nonadiabatic dissociation

---

\*Corresponding author. *Email address:* k1han@dicp.ac.cn (K.L.Han)

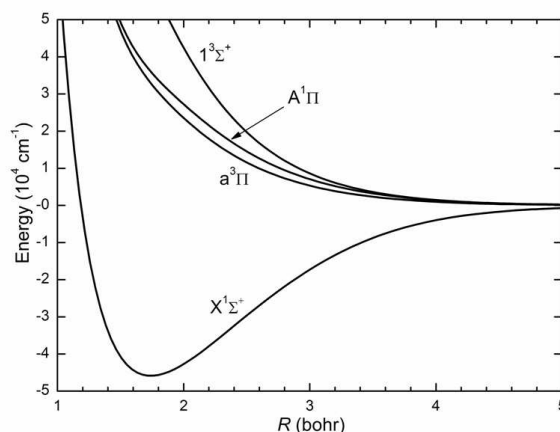
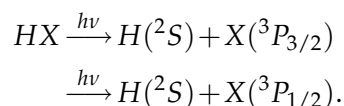


Figure 1: Diabatic potential energy curves for the  $X^1\Sigma^+$ ,  $a^3\Pi$ ,  $A^1\Pi$ , and  $^3\Sigma^+$  states as a function of the internuclear separation obtained from the ab initio calculation. The lower panel displays in more detail the long range feature of the curves.



Four electronic states ( $X^1\Sigma^+$ ,  $a^3\Pi$ ,  $A^1\Pi$ , and  $^3\Sigma^+$ ) are involved in the hydrogen halide photodissociation process (see, Fig. 1 for HF case), where ground state  $X^1\Sigma^+$  is the only bound one and the repulsive states  $a^3\Pi$ ,  $A^1\Pi$ , and  $^3\Sigma^+$  induce the fragmentation. Neglecting the spin-orbit coupling, all of the four states correlate with the lowest energy asymptote  $H(^2S)+X(^2P)$ . However, considering the nonadiabatic couplings among the dissociative channels either of the spin-orbit states,  $X(^2P_{3/2})$  and  $X(^2P_{1/2})$ , can be yielded, where  $X(^2P_{3/2})$  and  $X(^2P_{1/2})$  are ground and excited atomic spin-orbit states of the halogen fragment, respectively. Two sub-processes are included in the photodissociation process [9]: (i) initial excitation from the particular vibrational level of the ground electronic state to one (or more) of the repulsive states, and (ii) redistribution of the photodissociation flux via the nonadiabatic transitions between the accessible states. Most ground state of the closed-shell molecules are described by  $\Omega' = 0$  ( $\Omega$ , the projection of the electronic angular momentum along the molecular axis, can be used to classify the electronic states of diatomic molecules.); single-photon excitation can promote the molecule to excited states with  $\Omega = 0$  and  $\Omega = 1$  through parallel ( $\Delta\Omega = 0$ ) and perpendicular ( $\Delta\Omega = \pm 1$ ) excitations, respectively [10]. For the lighter halogen atom, i.e., F or Cl, the spin-orbit constant is small, the single electronic surface, i.e.,  $A^1\Pi$ , is often reached through the initial excitation [9, 11–15]. However, for the other heavier halogen atoms, Br, and I, since the spin-orbit constant is large, the excitation process is more complicated, where the spin-forbidden excitation can occur [9, 11]. The redistribution of dissociation flux among

the accessible states is the dynamic process where the nonadiabatic interactions play an important role. The relative yields of the spin-orbit states can provide the information about the initial excitation and the nonadiabatic transition of the flux. In this work relative yields is formulated by the branching fraction of the excited atomic fragment  $X^*$ ,

$$\Gamma = \frac{\sigma(X^*)}{\sigma(X^*) + \sigma(X)}, \quad (1)$$

where  $\sigma(X)$  and  $\sigma(X^*)$  are the partial cross-sections for ground and excited states of the halogen atoms, respectively.

Extensive investigations have been performed theoretically and experimentally for HCl [10, 16–27], HBr [23, 28–39], and HI [35, 40–50], including the studies where the reagents are created from the excited vibrational levels [16, 18, 21, 32, 41]. Especially, since HF and its deuterated counterpart have simpler configuration, different theoretical approaches have been employed to study their electronic structure and photodissociation dynamics [9, 12–15, 51–55]. Brown *et al.* [9] reported the first investigation of the spin-orbit branching fraction and total cross-section of HF and DF as the function of incident photon wavelength, where the molecular systems are initially excited from the vibrational level  $v=0$  of the ground electronic state and the time-dependent quantum wave packet treatment with the Chebychev propagation is employed. They also studied the vibrationally mediated photofragmentation with  $v=1, 2$  and 3 in their series paper [51], as well as the vector correlations and alignment parameters [52]. On the other hand, due to the experimental difficulties: HF is highly corrosive and its absorption lies in the vacuum ultraviolet (VUV) band starting at about 150 nm and peaking near 120 nm [56, 57], which corresponds to the  $A^1\Pi \leftarrow X^1\Sigma^+$  excitation as mentioned above, only a few experimental measurements were reported [11, 15, 56–59], where Zhang *et al.* [11] investigated the HF molecule initially excited to a single rotational level in the  $v=0$  and 3 vibrational state via IR (infrared) + VUV photolysis scheme and high- $n$  Rydberg time-of-flight (HRTOf) technique.

The goal of this work is to theoretically examine how the dissociative flux redistribute dynamically among the accessible electronic states and how the nonadiabatic interactions influence the fine structure of the fragments via the time dependent quantum approach with the split-operator scheme. The branching fractions are expected to be evaluated, compared with the experimental data and predicted for a broad range the incident photon energies. Section 2 presents the theory of the time-dependent wave packet treatment, with the Extended Split-Operator Scheme. The algorithm of the total and partial cross-sections is also given in this section. Section 3 indicates the *ab initio* calculations of potential energy curves (PECs), transition dipole moment and spin-orbit couplings. The results and analysis are reported in Section 4. The branching fractions and partial cross-section as the function of the photolysis wavelength and initial vibrational levels are exhibited in this section. The dynamic processes during the dissociation are also shown via the propagation of the wave packets. In the final section a brief conclusions is presented.

## 2 Theoretical method

### 2.1 Hamiltonian and Schrödinger equation

The time-dependent wave packet method is based on the solution of the time-dependent Schrödinger equation (Atomic units are used throughout the whole paper unless stated otherwise):

$$i\frac{\partial}{\partial t}\Phi(R,t) = H(R)\Phi(R,t), \quad (2)$$

where  $H(R)$  is the time-independent Hamiltonian of the molecular system, which is the sum of the nuclear kinetic energy operator  $T^N$ , electronic potential energy  $V(R)$  and the spin-orbit Hamiltonian  $H^{SO}(R)$

$$H(R) = T^N(R) + V(R) + H^{SO}(R), \quad (3)$$

where  $V(R)$  is the eigenvalue of the nonrelativistic electronic Born-Oppenheimer Hamiltonian, i.e., the potential in the diabatic representation,  $H^{SO}(R)$  is the spin-orbit operator in the Breit-Pauli approximation [60, 61], and  $T^N$  is the nuclear kinetic energy operator. For diatomic molecule  $T^N$  is given by

$$T^N(R) = -\frac{1}{2\mu R} \frac{\partial^2}{\partial R^2} R + \frac{\mathbf{I}^2}{2\mu R^2}, \quad (4)$$

where  $\mu$  is the reduced mass and  $\mathbf{I}$ , the relative orbital angular momentum of the nuclei, is given by

$$\mathbf{I} = \mathbf{J} - \mathbf{L} - \mathbf{S},$$

with  $\mathbf{J}$ ,  $\mathbf{L}$  and  $\mathbf{S}$  standing for the total, total electronic orbital, and total electron spin, angular momentum operators, respectively [61, 62]. The effect of rotation on the photodissociation dynamics was negligible in previous theoretical studies for HCl [16, 17, 20, 21] and HBr [28]. Consequently the  $\mathbf{I}^2$  term is neglected in the present work.

### 2.2 Initial wave packet

Based on the time-dependent framework, the initial wave packet is prepared to satisfy the initial condition [63–68]

$$\Phi(R, t=0) = \mu(R)\Psi(R), \quad (5)$$

i.e., the initial wave packet is the product of the transition dipole moment  $\mu(R)$  and the nuclear wave function  $\Psi(R)$  of the ground state. Here  $\mu(R)$  is a single component of a

spherical vector. For an  $n$ -state system, Eq. (5) is expressed in the matrix form by

$$\begin{pmatrix} \Phi_1(R, t=0) \\ \Phi_2(R, t=0) \\ \vdots \\ \Phi_n(R, t=0) \end{pmatrix} = \begin{pmatrix} \mu_1(R)\Psi(R) \\ \mu_2(R)\Psi(R) \\ \vdots \\ \mu_n(R)\Psi(R) \end{pmatrix}. \quad (6)$$

As commented above, photodissociation of HF can be treated as a three-state problem involving  $a^3\Pi$ ,  $A^1\Pi$ , and  $^3\Sigma^+$  states, where the states are labeled in Hund's case (a) approximation and the  $\Omega=1$  component out of the three components ( $\Omega=0, 1$  and  $2$ ) is considered in this calculation. Hence the initial column wave packet for HF is given in the diabatic representation by

$$\begin{pmatrix} \Phi_1(R, t=0) \\ \Phi_2(R, t=0) \\ \Phi_3(R, t=0) \end{pmatrix} = \begin{pmatrix} 0 \\ \mu(R)\Psi(R) \\ 0 \end{pmatrix}, \quad (7)$$

where  $\mu(R)$  is the transition dipole moment for the  $A^1\Pi \leftarrow X^1\Sigma^+$  transition which is the only initial excitation occurring in the diabatic representation, and  $\Psi(R)$  is the wave function of particular vibrational level on the ground electronic state.

### 2.3 Propagation of the wave packet

The formal solution to Eq. (2) is

$$\Phi(R, t) = \exp(-iHt)\Phi(R, t=0), \quad (8)$$

where  $\exp(-iHt)$  is the time-evolution operator, which is used in the time-dependent method to propagate the wave packets in a series of short time steps. To obtain the numerical solution of Eq. (8), the split-operator scheme [69, 70] has been modified and then extended for treating the propagation involving multiple electronic states [71–84]. For each time step  $\Delta$ , the wave packet propagation for the three-state problem can be described in the matrix form as

$$\begin{pmatrix} \Phi_1(R, t+\Delta) \\ \Phi_2(R, t+\Delta) \\ \Phi_3(R, t+\Delta) \end{pmatrix} = \exp\left(-i\mathbf{T}\frac{\Delta}{2}\right) \exp\left(-i \begin{pmatrix} U_{11}(R) & U_{12}(R) & U_{13}(R) \\ U_{21}(R) & U_{22}(R) & U_{23}(R) \\ U_{31}(R) & U_{32}(R) & U_{33}(R) \end{pmatrix} \Delta\right) \\ \times \exp\left(-i\mathbf{T}\frac{\Delta}{2}\right) \begin{pmatrix} \Phi_1(R, t) \\ \Phi_2(R, t) \\ \Phi_3(R, t) \end{pmatrix}, \quad (9)$$

where  $U(R)$  is the effective potential energy matrix defined as

$$U(R) = V(R) + H^{SO}(R).$$

The effective matrix can be diagonalized as

$$\begin{bmatrix} U_{11}(R) & U_{12}(R) & U_{13}(R) \\ U_{21}(R) & U_{22}(R) & U_{23}(R) \\ U_{31}(R) & U_{32}(R) & U_{33}(R) \end{bmatrix} = \mathbf{M}^T(R) \begin{bmatrix} U_1(R) & 0 & 0 \\ 0 & U_2(R) & 0 \\ 0 & 0 & U_3(R) \end{bmatrix} \mathbf{M}(R), \quad (10)$$

where  $\mathbf{M}(R)$  is the unitary matrix determined via diagonalizing the potential matrix, and  $\mathbf{M}^T(R)$  is the transpose matrix of  $\mathbf{M}(R)$ . Hence, Eq. (9) can be reformed as

$$\begin{bmatrix} \Phi_1(R, t + \Delta) \\ \Phi_2(R, t + \Delta) \\ \Phi_3(R, t + \Delta) \end{bmatrix} = \exp\left(-i\mathbf{T}\frac{\Delta}{2}\right) \times \mathbf{M}^T(R) \{\mathbf{D}\} \mathbf{M}(R) \exp\left(-i\mathbf{T}\frac{\Delta}{2}\right) \begin{bmatrix} \Phi_1(R, t) \\ \Phi_2(R, t) \\ \Phi_3(R, t) \end{bmatrix}, \quad (11)$$

where  $\{\mathbf{D}\}$  is a diagonal matrix of the form

$$\{\mathbf{D}\} = \text{diag}\left(\exp[-iU_1(R)\Delta], \exp[-iU_2(R)\Delta], \exp[-iU_3(R)\Delta]\right).$$

It should be noted that two representation are employed in the investigation of nonadiabatic process [1, 9, 21, 61, 71]: (i) the diabatic representation, corresponding the diabatic electronic basis, in which  $S^2$ ,  $\Lambda$ , and  $\Sigma$ , are good quantum numbers and the effective potential matrix  $\mathbf{U}(R)$  has off-diagonal elements, which causing the transitions between the considered states, and (ii) the adiabatic representation, corresponding to the adiabatic electronic basis, in which  $\Omega$  is the only good quantum number, the effective potential matrix is diagonal, and the interactions between adiabatic states result from the off-diagonal terms in the kinetic operator  $T^N$ . Based on the relationship between the diabatic and adiabatic representation, the matrix  $\mathbf{M}(R)$  in Eq. (10) is the diabatic-to-adiabatic transformation matrix [1]. Consequently, the wave packet on the  $j$ th adiabatic state can be expressed as a superposition over the ones on the diabatic states

$$\Phi_j^{ad}(R) = \sum_j m_{ji}(R) \Phi_i^{diab}(R), \quad (12)$$

where  $m_{ji}(R)$  is the element of the transformation matrix  $\mathbf{M}(R)$ . Nevertheless, it should be noted that the labels of the states in the adiabatic representation have no physical significance, because the fully adiabatic states are the superposition of the diabatic states,

$$\begin{pmatrix} U_1^{ad}(R) & 0 & 0 \\ 0 & U_2^{ad}(R) & 0 \\ 0 & 0 & U_3^{ad}(R) \end{pmatrix} = \mathbf{M}(R) \begin{pmatrix} U_{11}(R) & U_{12}(R) & U_{13}(R) \\ U_{21}(R) & U_{22}(R) & U_{23}(R) \\ U_{31}(R) & U_{32}(R) & U_{33}(R) \end{pmatrix} \mathbf{M}^T(R). \quad (13)$$

The wave packet and potential curve associated with the adiabatic state in the following parts of this paper will be designated by the good quantum number  $\Omega$  and the label of the diabatic state which makes the majority contribution to the adiabatic one in the Franck-Condon region, i.e., has the largest coefficient  $m_{ji}(R)$  [9].

As a practical calculation, the propagation of wave packets is performed in the diabatic representation. The sine-basis DVR is employed to treat the coordinate  $R$  as applied in other scattering/half-scattering problems [85–87]. The complex absorbing potential is added at the edge of grid to avoid the boundary reflection of the wave packets [88–90].

## 2.4 Final states analysis

Both diabatic and adiabatic models are useful when discussing dissociative dynamics. But the physically meaningful results are obtained in the adiabatic representation. To calculate the branching fraction, and subsequently compare it with the experimental data, the adiabatic wave packet on each dissociative channel is necessary. Since the propagation presented in Section 2.3 is performed in diabatic representation, the wave packets must be transformed into the adiabatic representation before the final-state analysis. The matrix form of Eq. (12) is taken to obtain the adiabatic wave packets.

The algorithm of partial cross-section has been established to investigate photodissociation [5, 66, 91]. By detecting the wave packet on the adiabatic state at  $R = R_\infty$ , locating in the asymptotic region where no further couplings exist among the involved states, the partial cross-section for the  $j$ th product channel are formulated in SI unit as,

$$\sigma_j(\nu) = \left( \frac{4\pi^3 \nu k_j}{3c\epsilon_0 \mu} \right) |A_j(R_\infty, E)|^2, \quad (14)$$

where

$$A_j(R_\infty, E) = \frac{1}{2\pi} \int_0^\infty \Phi_j(R_\infty, t) \exp[i(E_{ini} + h\nu)t/\hbar] dt, \quad (15)$$

$\nu$  is the incident photon frequency,  $\mu$  is reduced mass of the fragments,  $c$  is the velocity of light in vacuum,  $\epsilon_0$  is the permittivity in free space,  $E_{ini}$  is initial state energy, and  $k_j$  is the wave vector for the  $j$ th channel and can be expressed as [44, 91]

$$k_j = \left[ \frac{2\mu}{\hbar^2} (E_{ini} + h\nu - \epsilon_j) \right]^{\frac{1}{2}} = \left[ \frac{2\mu}{\hbar^2} (E_{ini} + h\nu - U_j(R_\infty)) \right]^{\frac{1}{2}}, \quad (16)$$

with  $U_j(R_\infty)$  standing for the value of the adiabatic potential at  $R = R_\infty$ . The calculated partial cross-sections are subsequently used to attain the branching fractions from Eq. (1).

The approach for the total cross-section has also been developed and applied for the final-state analysis [63–68]. The total cross-section at the particular incident radiation is given by the time-energy Fourier transform of the autocorrelation function in the SI unit,

$$\sigma_{tot}(\nu) = \frac{2\pi\nu}{3c\epsilon_0} \int_0^\infty \exp[i(E_{ini} + h\nu)t/\hbar] A(t) dt, \quad (17)$$

where the total autocorrelation function  $A(t)$  is accumulated with respect to the wave packets over the grids and summed including all the considered states at each time step,

$$A(t) = \sum_{j=1}^n \int_{R_{min}}^{R_{max}} \Phi_j^*(R, t=0) \Phi_j(R, t) dR. \quad (18)$$

### 3 *Ab initio* calculation

Four electronic states,  $X^1\Sigma^+$ ,  $a^3\Pi$ ,  $A^1\Pi$ , and  $^3\Sigma^+$ , are involved in the photodissociation study of HF and DF, where  $X^1\Sigma^+$  is the only bond state and  $a^3\Pi$ ,  $A^1\Pi$ , and  $^3\Sigma^+$  are the

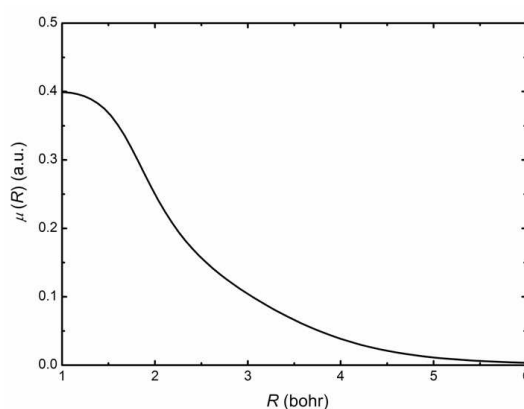


Figure 2: The transition dipole moment for the excitation  $A^1\Pi \leftarrow X^1\Sigma^+$  as a function of internuclear distance obtained from the *ab initio* calculation.

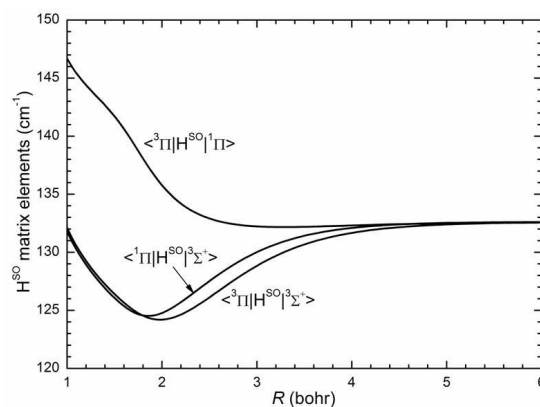


Figure 3: Dependence on the internuclear distance of the spin-orbit couplings matrix elements from the *ab initio* calculation

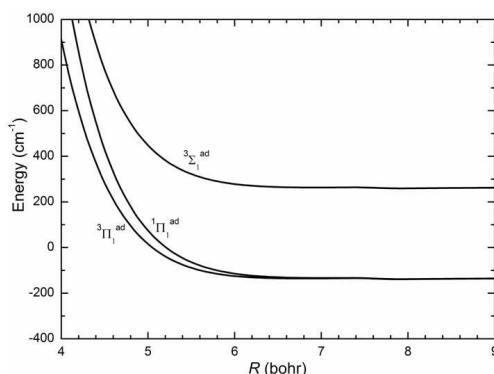


Figure 4: Fully adiabatic potential energy curves as function of internuclear distance obtained via Eq. (13). Note that only the  $\Omega=1$  manifold is considered in the present calculation, and the states are labeled by the quantum number  $\Omega$  and the diabatic state with the largest contribution in the Franck-Condon region.

repulsive states involved in the dissociation. The diabatic potential energies of HF for all the data points of internuclear separation are calculated using multi-reference configuration interaction (MRCI) scheme with augmented correlation-consistent polarized valence 6-zeta (aug-cc-pv6z) basis set and the symmetry of  $C_{2v}$ . The MRCI calculations are based on state-averaged complete active space self-consistent field (SA-CASSCF) calculation, where the states,  $^1\Sigma^+$ ,  $^3\Sigma^+$ ,  $^1\Pi_x$ ,  $^1\Pi_y$ ,  $^3\Pi_x$  and  $^3\Pi_y$ , correlating with the lowest energy asymptote,  $H(^2S) + F(^2P)$ , are included. The active space was chosen to consist of eight electrons in five orbitals ( $3a_1, 1b_1, 1b_2$ ). The diabatic PECs are presented in Fig.1.

Since the  $A^1\Pi \leftarrow X^1\Sigma^+$  is the only allowed transition in the initial excitation, the transition dipole moment connecting these two states is computed and illustrated as a function of internuclear distance in Fig. 2.

Fig. 3 depicts the dependence of R of the spin-orbit coupling matrix elements among the considered states. a common set of the orbitals and wave functions are firstly calculated via SA-CASSCF approach, then are used to obtain the  $H^{SO}$  matrix elements via the spin-orbit operator in the Breit-Pauli approximation [60]. The evaluated spin-orbit splitting between the fluorine asymptotes is equal to  $398.0 \text{ cm}^{-1}$ , which is in good accord with the experimental data  $404.1 \text{ cm}^{-1}$  [92].

The fully adiabatic potentials can be obtained from Eq. (13). The adiabatic states are labeled by the good quantum number  $\Omega$  and the diabatic states which make the largest contributions to the adiabatic ones in Franck-Condon region. The  $\Omega=1$  component are shown in Fig. 4. It is clear that the  $^3\Pi_1^{ad}$  and  $^1\Pi_a^{ad}$  states correlate adiabatically with the asymptote of the ground fluorine atom  $F(^2P_{3/2})$ , while the  $^3\Sigma_1^{ad}$  leads to the production of the excited fluorine atom  $F(^2P_{1/2})$ .

All the electronic structure calculations are performed using the MOLPRO suite of quantum chemistry program [93].

## 4 Results and discussion

As commented in Section I two processes are involved in present calculation: initial excitation and flux redistribution. In this work the initial excitation only occurs between  $X^1\Sigma^+$  and  $A^1\Pi$  diabatic states. As presented in Fig. 4 the fully adiabatic state  $^1\Pi_1^{ad}$  correlates with the ground fluorine atomic state  $F(^2P_{3/2})$ . Therefore, if no flux transition occurs during the dissociation, the excited state branching fraction of the excited fluorine spin-orbit fine-structure would be zero. Former theoretical [9, 51] and experimental [11] treatments have reported the non-zero spin-orbit branching fraction of the excited fluorine spin-orbit state  $F(^2P_{1/2})$ , which imply that the flux substantially redistributes during the dissociative process. The goal of this work is to examine theoretically how the dissociative flux redistributes among the considered states via nonadiabatic interactions and how the branching fractions of the fragment reflect the contributions from the accessible states.

### 4.1 Nonadiabatic transitions during propagation

The diabatic-to-adiabatic transformation matrix  $\mathbf{M}(R)$  from Eq. (10) is a signature of the nonadiabatic interactions which control the mixture of the flux among the different dissociative channels. It exhibits the contributions of the diabatic states to the adiabatic ones. The elements of the matrix, i.e., the coefficients of the contribution are displayed as

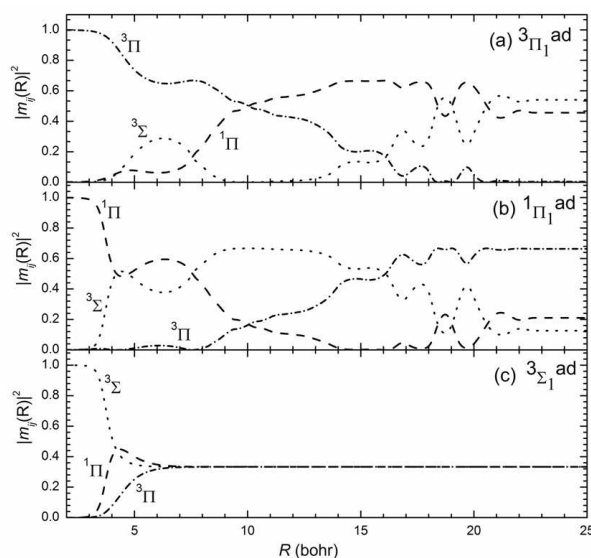


Figure 5: The contribution  $|m_{ji}(R)|^2$  of the diabatic states  $^3\Pi$  (dot-dash line),  $^1\Pi$  (dashed line), and  $^3\Sigma$  (dot line) to the fully adiabatic states, (a)  $^3\Pi_1^{ad}$ , (b)  $^1\Pi_1^{ad}$ , and (c)  $^3\Sigma_1^{ad}$ , as a function of internuclear distance. The states are labeled by the quantum number  $\Omega$  and the diabatic state with the largest contribution in the Franck-Condon region.

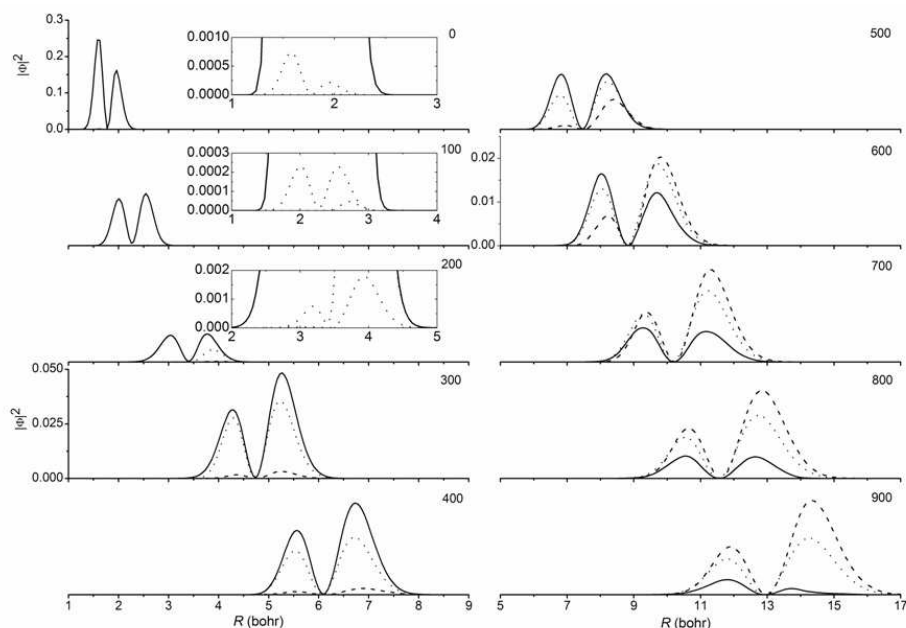


Figure 6: The snapshots of the propagating adiabatic wave packets for HF ( $v=1$ ) at various time steps from  $t = 0$  a.u. to 900 a.u. The wave packets are labeled by the diatomic component making the largest contribution to the adiabat:  ${}^1\Pi_1^{ad}$  (dashed line);  ${}^1\Pi_1^{ad}$  (solid line);  ${}^3\Sigma_1^{ad}$  (dotted line). The amplitudes of the wave packet are scaled on the arbitrary unit. The vertical axes of the plots at  $t \leq 200$  should be referred to the one at  $t = 0$ , the ones at  $t = 300-500$  to  $t = 300$ , and the ones at  $t \geq 600$  to  $t = 600$ . The insets show the small separation behavior in more detail.

the function of bond separation in Fig. 5. In the Franck-Condon region there are almost no changes of the coefficients, which means no obvious mixing between triplet states and the initial created singlet state and also verifies the assumption that initial excitation occurs only between  $X^1\Sigma^+$  and  $A^1\Pi$  states. The sharp variation indicating the dramatic mixture of the flux starts at about  $R = 3$  bohr. The coefficients vary substantially over a broad range ( $R \sim 3-10$  bohr), where the nonadiabatic interactions substantially influence the flux distribution of the dissociative channels. In the asymptotic region the coefficients still have the nonzero magnitudes, which implies that the established flux is still being redistributed by the asymptotic couplings, although the mixing is not as significant as in the previous area.

One of the advantages of time dependent wave packet approach is that the distribution of the dissociative flux for each channel can be directly elucidated though the motion of the corresponding wave packet. For example, the snapshots of the adiabatic wave packets for HF and DF in  $v = 1$  cases are delineated in Figs. 6 and 7, respectively. The time unit is a.u., the squared amplitudes  $|\Phi|^2$  are plotted as arbitrary unit, and the

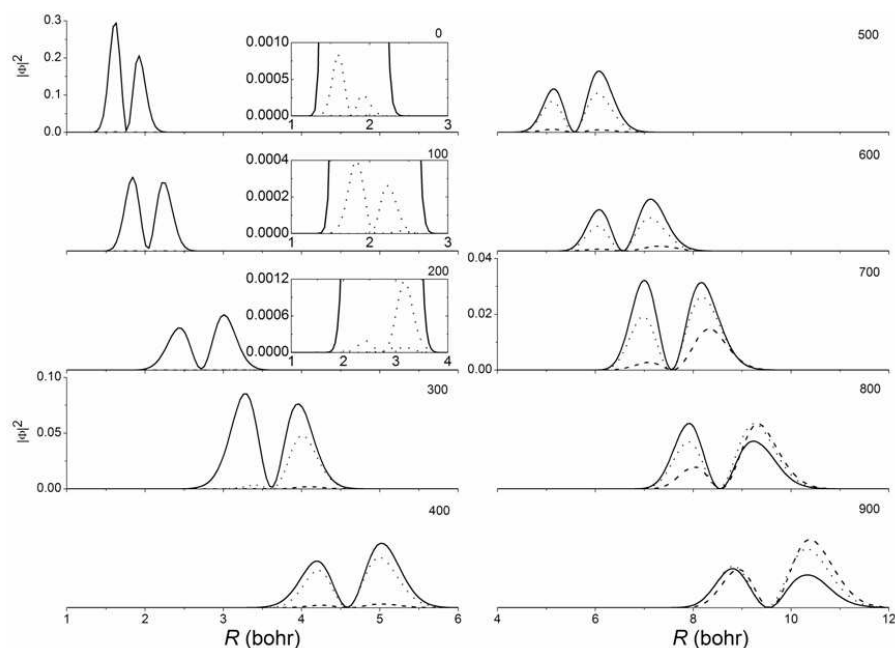


Figure 7: The analogous plot to Fig. 6 for DF ( $v=1$ ). The vertical axes of the plots at  $t \leq 200$  should be referred to the one at  $t = 0$ , the ones at  $t = 300-600$  to  $t = 300$ , and the ones at  $t \geq 700$  to  $t = 700$ .

vertical axes are expanded at some steps. For comparison the time dependent norm  $|\langle \Phi_j(R,t) | \Phi_j(R,t) \rangle|^2$  of the wave packet on  $j$ th adiabatic state are evaluated in the same cases and plotted in Fig. 8. At the beginning of the time step the wave packet lies predominately on the adiabatic  ${}^1\Pi_1^{ad}$  state. In the earlier stage (about 100 a.u. for HF in Fig. 6 and 200 a.u. for DF in Fig. 7) the wave packets still stay in the Franck-Condon area, and there is no obvious population on the adiabatic triplet states. This is consistent with behavior of the time dependent probabilities at the short time realm of Fig. 8. At that time the dissociation does not start, and there is no significant transfer of the flux from the initially populated  ${}^1\Pi$  states to the triplet states. It is also verified by the feature of the contribution coefficients  $m_{ji}(R)$  in Franck-Condon region in Fig. 5. At the sequent time steps the dramatic changes appear during the propagation (see, around 200 a.u. for HF in Fig. 6 and 300 a.u. for DF in Fig. 7). This is also proved by the behavior of the probabilities at the corresponding time in Fig. 8. The populations on the triplet states are fast established, while the wave packet on the  ${}^1\Pi_1^{ad}$  state drops sharply, which, however, is still the major component. It implies that the flux is substantially redistributed among the adiabatic channels. Especially, the probability on the  ${}^3\Sigma_1^{ad}$  state, which adiabatically correlating with excited fluorine atom product, exhibits a sharp rise in Fig.8. Meanwhile, the expansion of the molecular separation is obvious, and the wave packets arrival at the internuclear separation between 3 bohr and 5 bohr. Comparing with the variation of the

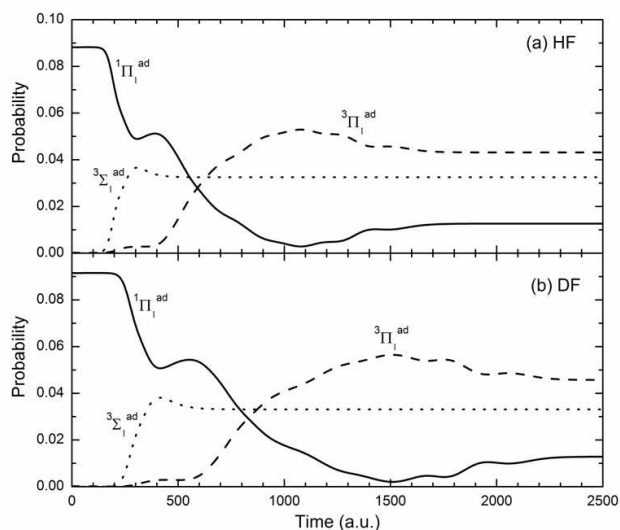


Figure 8: Time dependent norm as a function of time for HF (upper panel) and DF (lower panel) with initial excitation from  $v=1$ . The probability is scaled on arbitrary unit.

contribution coefficients in Fig. 5, which present the sharp variation in the same area, the redistribution of the flux seems reasonable and can be interpreted to arise from the spin-orbit couplings in diabatic representation or the off-diagonal elements of the kinetic operator in adiabatic representation. As continue evolving with time, the wave packet on  $^1\Pi_1^{ad}$  state keeps decreasing while the populations on the adiabatic triplet states keep rising. It should be noted from Fig. 8 that the probability on  $^3\Sigma_1^{ad}$  state has reach its stable value at about 500 a.u. for HF and 600 a.u. for DF, respectively. It can also be verified via Fig. 5 (c) where the contribution from the diabatic states to the  $^3\Sigma_1^{ad}$  state has already reach their asymptotic values even at the small internuclear distance ( $R \sim 7$  bohr). At about 600 a.u. for HF and 800 a.u. for DF in Fig. 8, the amplitudes of the three states have comparable weight and the wave packets is roughly passing the internuclear separation of 9-10 bohr as shown in Figs. 6 and 7. After that the population on  $^1\Pi_1^{ad}$  state keeps decreasing and the triplet states become the larger component. In Fig. 8 the probability on  $^3\Sigma_1^{ad}$  retains its asymptotic value, while the variations are still shown on  $^3\Pi_1^{ad}$  and the  $^1\Pi_1^{ad}$  states. Since both  $^3\Pi_1^{ad}$  and the  $^1\Pi_1^{ad}$  states correlate with the ground fluorine product, switching of the flux between the two states will not influence the branching fraction of the fragments but only affect the partial cross sections.

Moreover, contrasting the behavior of the wave packets and the variation of probabilities for HF and DF in Figs. 6-8, it seems that the overall velocity of the wave packets for HF is larger than its deuterated counterpart, i.e., the one with the lighter mass has larger dissociative rate. It can also be understood as the influence of the kinetic energy operator  $T^N$  [21, 44]. The kinetic energy operator take the derivative form regarding the internu-

clear coordinate and describe the motion of the wave packets from the Franck-Condon region to the asymptotic area, i.e., it drives the wave packets moving along the adiabatic potentials. On the other hand, transitions between the adiabatic states arise from the off-diagonal terms of the kinetic energy operator and the redistributive flux is substantially affected by these terms in the adiabatic representation.

The evolution process of the wave packets gives a clear physical picture of the flux redistribution as the break-up of the molecule. Combining with the feature of the contribution coefficients of diabatic states to adiabatic states in Fig. 5 and the wave packet propagation in Figs. 6 and 7, it can be concluded that the nonadiabatic interactions in three distinct regions influence the dissociative process as demonstrated in other molecules [9,94–97]. The molecule is initially excited in the Franck-Condon region, where the separations between the potentials are large and there are no significant interactions between the states. The dissociative flux is established on  $^1\Pi$  state, which dominates over the total flux. At larger internuclear distance (recoupling zone, about 3-10 bohr), where the inter-state separations are comparable to the spin-orbit couplings, the nonadiabatic transitions substantially influence the behavior of the wave packets and redistribute the flux established in the Franck-Condon region. At the largest distance (asymptotic region), where the potential energies almost reach their asymptotic magnitudes, the nonadiabatic couplings (asymptotic spin-orbit coupling) still exists and lift the degeneracy of the atomic multiplet and affect the product spin-orbit branching fraction [9,94].

## 4.2 Cross sections and branching fractions

The total cross sections are evaluated via Eq. (17) over a large incident photon energy region. Included in Fig. 9 are the total cross sections for HF and DF with  $v=0-3$ . These absorption spectra are broad and featureless, indicating a prompt dissociation. For both

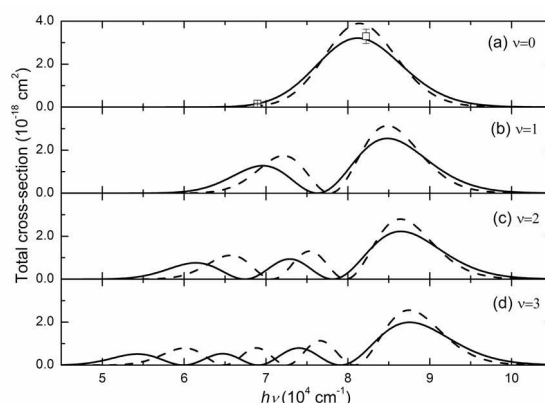


Figure 9: Total cross section as function of incident photon energy for HF (solid line) and DF (dashed line) with  $v=0-3$ . Also shown is the experimental value (squares) for HF ( $v=0$ ) from Nee *et al.* [57].

Table 1: Maxima and minima in branching fractions and minima in partial cross-sections for HF initially excited from  $v=0-3$ . Energies of incident photon are given in  $\text{cm}^{-1}$ .  $\Gamma$  is the branching fraction for excited fluorine atomic product.  $\sigma$  is the partial cross-section for each adiabatic state.

Vibrational level		Minima		High-energy maxima			Low-energy maxima <sup>a</sup>	
0	$\Gamma$						54539 (0.444)	
1	$\Gamma$	76182			76483		50180 (0.432)	
	$\sigma(^3\Pi_1^{ad})$	76182						
	$\sigma(^1\Pi_1^{ad})$	76633						
	$\sigma(^1\Sigma_1^{ad})$	76182						
2	$\Gamma$	67314	77986	67615	78287		46122 (0.421)	
	$\sigma(^3\Pi_1^{ad})$	67465	78136					
	$\sigma(^1\Pi_1^{ad})$	67615	78437					
	$\sigma(^1\Sigma_1^{ad})$	67314	77986					
3	$\Gamma$	59800	68968	78888	60100	69118	79339	42064 (0.410)
	$\sigma(^3\Pi_1^{ad})$	59950	69118	79038				
	$\sigma(^1\Pi_1^{ad})$	60100	69269	79339				
	$\sigma(^1\Sigma_1^{ad})$	59800	68968	79038				

<sup>a</sup>The magnitudes of the low-energy maxima is given in parenthesis.

Table 2: Maxima and minima in branching fractions and minima in partial cross-sections for DF initially excited from  $v=0-3$ . Energies of incident photon are given in  $\text{cm}^{-1}$ .  $\Gamma$  is the branching fraction for excited fluorine atomic product.  $\sigma$  is the partial cross-section for each adiabatic state.

Vibrational level		Minima		High-energy maxima			Low-energy maxima <sup>a</sup>	
0	$\Gamma$						53937 (0.537)	
1	$\Gamma$	77685			77986		50631 (0.530)	
	$\sigma(^3\Pi_1^{ad})$	77836						
	$\sigma(^1\Pi_1^{ad})$	77985						
	$\sigma(^1\Sigma_1^{ad})$	77685						
2	$\Gamma$	70621	79639	70922	79940		47475 (0.521)	
	$\sigma(^3\Pi_1^{ad})$	70771	79790					
	$\sigma(^1\Pi_1^{ad})$	70922	79940					
	$\sigma(^1\Sigma_1^{ad})$	70772	79639					
3	$\Gamma$	64760	72425	80691	65060	72725	80992	44319 (0.511)
	$\sigma(^3\Pi_1^{ad})$	64910	72425	80842				
	$\sigma(^1\Pi_1^{ad})$	65060	72725	81142				
	$\sigma(^1\Sigma_1^{ad})$	64910	72425	80691				

<sup>a</sup>The magnitudes of the low-energy maxima is given in parenthesis.

HF and DF the highest peaks shift to the large energies with increasing the vibrational levels. Comparing the plots of the HF and DF cases, the total cross sections of DF present the narrower envelop and the larger peak magnitude which also locate at the higher

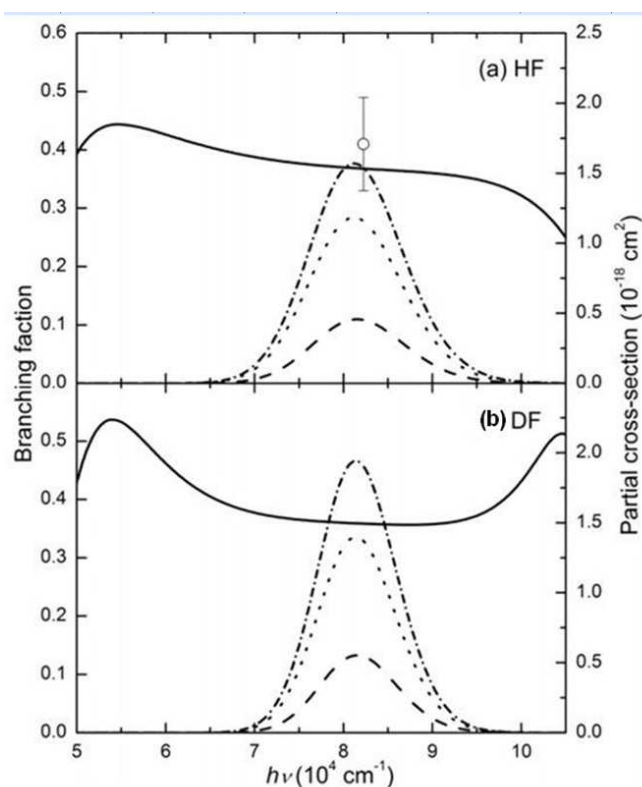


Figure 10: Branching fractions (solid line) and partial cross-sections on adiabatic state  $^3\Pi_1^{ad}$  (dot-dash line),  $^1\Pi_1^{ad}$  (dashed line) and  $^3\Pi_1^{ad}$  (dotted line) as a function of incident photon energies with initial excitation from  $v = 0$  vibrational level for (a) HF and (b) DF. Also shown is the experimental value (circle) of the branching fraction for HF at 121.6 nm ( $82237 \text{ cm}^{-1}$ ) from Zhang *et al.* [11].

energies. The calculated total cross sections for HF ( $v=0$ ) case at 121.6 nm and 145 nm are  $3.15 \times 10^{-18} \text{ cm}^2$  and  $1.65 \times 10^{-19} \text{ cm}^2$ , respectively, which are in excellent agreement with the experimental measurement  $3.3 \times 10^{-18} \text{ cm}^2$  (121.6 nm) and  $1.7 \times 10^{-19} \text{ cm}^2$  (145 nm) from Nee *et al.* [57].

The branching fractions for HF and DF from Eq. (1) in the adiabatic representation with initial excitation from vibrational levels  $v = 0-3$  are displayed as the function of incident photon energies in Figs. 10-13, respectively, as well as the partial cross-section from Eq. (14) for each adiabat. The experimental branching fractions,  $0.41 \pm 0.08$  for HF ( $v=0$ ) at 121.6 nm and  $0.42 \pm 0.03$  for HF ( $v=3$ ) at 193.3 nm, are reported by Zhang *et al.* [11]. Present calculated values at these two cases are 0.368 and 0.367, respectively, which reveal the good accord with the experimental data.

There are several common features for HF and DF in these plots. The branching fraction shows a maximum at the lower excitation frequencies in each case (also see Tables 1 and 2). The magnitude of the maximum for DF is always larger than HF regarding the

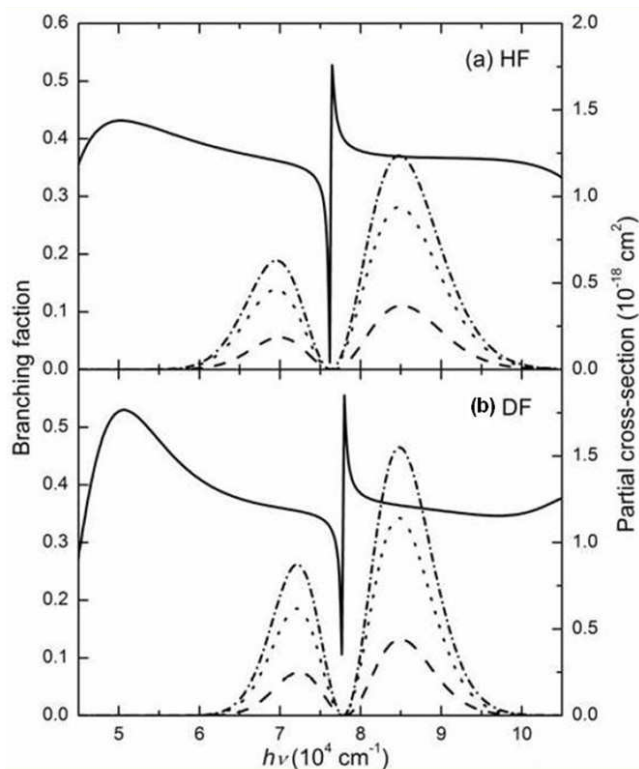


Figure 11: An analogous plot to Fig. 10 with excitation of  $v=1$  vibrational level.

same initial vibrational level. With the vibrational level changing from  $v=0$  to 3 the position of this maximum shifts to the lower energy and the decreasing of its magnitude is also revealed. This shifting feature of the branching fraction was interpreted by Brown *et al.* from two aspects [51]: the molecule need less excitation energy to be promoted to the repulsive states, and the ground state vibrational wave function with larger vibrational quantum number has substantial amplitude at larger internuclear separations where the energy separation between the ground and excited states is smaller. The height of the low-energy maximum decreases with increasing the vibraional levels, which is presented in Tables 1 and 2.

The oscillatory behavior appears in both the partial cross-sections and branching fractions of the  $v=1-3$  cases, where the number of the minima is equal to the nodal number of the vibrational wave function of the ground electronic states, i.e., one for  $v=1$ , two for  $v=2$ , and three for  $v=3$ . In the  $v=0$  case there is no minimum value/oscillation of the partial cross-section and branching fraction, but it can still be generalized into the nodal pattern. That is, the number of the minima is zero, which corresponds to zero node of the  $v=0$  level of the ground electronic state. It implies that the nodal pattern can be understood as the transfer of the nodal feature of the ground states vibrational wave function

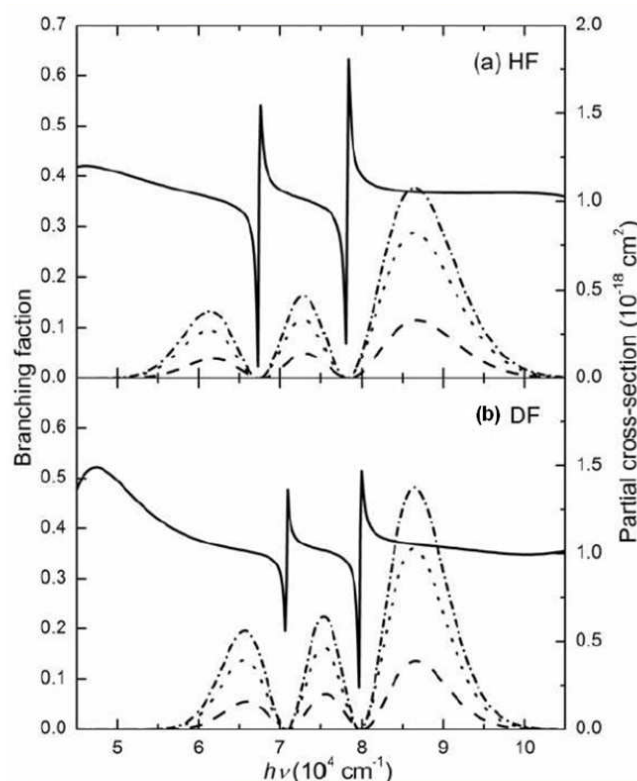


Figure 12: An analogous plot to Fig. 10 with excitation of  $v=2$  vibrational level.

as it is initially excited into the repulsive state and then carried into other states via the nanadiabatic interaction [21]. Tables 1 and 2 also presents the frequencies where the minima of partial cross-sections and branching fractions of HF and DF reach the minima and maxima, respectively. The appearance of the minima of partial cross-sections can be interpreted by the reflection principle [1, 51, 98], while the occurring position of the minima and the concomitant maxima (which are referred to the higher-energy maxima in Tables 1 and 2 and following part of this paper to distinguish with the lower-energy maxima discussed above). of the branching fractions, even the energy ordering of them, is still in argument for hydrogen halides and their deuterated species [16, 17, 21, 51]. From the fully adiabatic potentials depicted in Fig. 4, it is clear that the excited fluorine  $F^*$  atom product arises from the adiabatic channel  $^3\Sigma_1^+$ , while  $^3\Pi_1$  and  $^1\Pi_1$  states lead to the ground fluorine channel. However, with a close inspection in Tables 1 and 2, the partial cross-sections  $^3\Pi_1$  and  $^1\Pi_1$  states do not reach their minima at the same frequency. The interplay between these two cross-sections results in the fact that the branching fraction of ground F atom channel drop to its minimum at the different frequency. Furthermore, it is also attributed to the inconsistency of the position of the branching fraction and the partial cross-section correlating with the excited  $F^*$  atomic channel. The magnitudes of

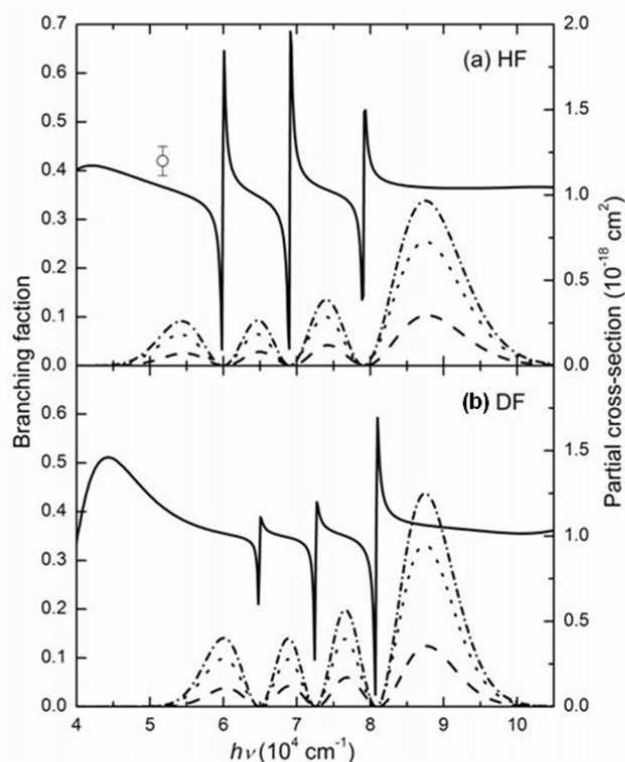


Figure 13: An analogous plot to Fig. 10 with excitation of  $v=3$  vibrational level. Also shown is the experimental value (circle) of the branching fraction for HF at 193.3 nm ( $51733\text{ cm}^{-1}$ ) from Zhang *et al.* [11].

the minima and maxima of the branching fractions are also influenced by the divergence of the partial cross-sections.

## 5 Summary and conclusions

Photodissociation of hydrogen fluoride and its deuterated species includes initially creation from the particular vibrational level of the ground electronic state  $X^1\Sigma^+$  and subsequent fragmentation induced by the repulsive states  $^3\Pi$ ,  $^1\Pi$ , and  $^3\Sigma^+$ . The photodissociation process is treated as the three-state problem and investigated using the time-dependent quantum wave packet approach with the split-operator propagation scheme. The dynamic process is studied based on the accurate *ab initio* calculation of the PECs, transition dipole moment and the spin-orbit couplings among the accessible states. The evolution of the wave packet and dissociative flux is presented. Taking the advantage of the wave packet approach, a clear physical picture is exhibited for the dissociative process. Nonadiabatic interactions, especially the spin-orbit couplings, play an important role in determining the flux distribution, which can be reflected by the branching

fraction of fine-structure of the fluorine fragment. The total cross-sections, partials cross-sections and branching fractions as a function of incident photon energies for both HF and DF initially excited from the vibrational levels  $v=0-3$  are evaluated and compared with the available experimental data. The oscillatory behavior is revealed in both of the partials cross-sections and the branching fractions. The divergence of the frequencies where the partials cross-sections and the branching fractions reach their minima, as well as the magnitudes of the minima and maxima of branching fractions, can be interpreted by the interplays among the positions of the minima of partial cross-sections. The agreement of the present work with the previous experimental and theoretical results indicates the reliability of the *ab initio* calculation and dynamic approaches in this work. The calculated total cross sections for HF ( $v=0$ ) case at 121.6 nm and 145 nm are  $3.15 \times 10^{-18}$  cm<sup>2</sup> and  $1.65 \times 10^{-19}$  cm<sup>2</sup>, respectively, which are in excellent agreement with the measurement  $3.3 \times 10^{-18}$  cm<sup>2</sup> (121.6 nm) and  $1.7 \times 10^{-19}$  cm<sup>2</sup> (145 nm) by Nee *et al.* [57]. The calculated branching fractions of HF, which are equal to 0.368 at 121.6 nm for  $v=0$  case and 0.367 at 193.3 nm for  $v=3$  case, accord well with the experimental data  $0.41 \pm 0.08$  and  $0.42 \pm 0.03$  from Zhang *et al.*, respectively [11]. The prediction of the branching fractions covering a broad range of the frequencies for both HF and DF is also illustrated in this paper. It is hoped that these results will be beneficial to resolve the discrepancies between the experimental and computational results, especially at the wave lengths where the experimental measurement has not been available.

**Acknowledgements.** The authors would like to acknowledge the helpful advice of Prof. G. G. Balint-Kurti.

## References

- [1] R. Schinke, *Photodissociation Dynamics: Spectroscopy and Fragmentation of Small Polyatomic Molecules* (Cambridge University Press, Cambridge, 1993).
- [2] R. N. Dixon, *Acc. Chem. Res.* 24 (1991) 16.
- [3] S. J. Singer, K. F. Freed, and Y. B. Band, *Adv. Chem. Phys.* 61 (1985) 1.
- [4] G. G. Balint-Kurti and M. Shapiro, *Adv. Chem. Phys.* 60 (1985) 403.
- [5] G. G. Balint-Kurti, *Adv. Chem. Phys.* 128 (2004) 249.
- [6] P. Brumer and M. Shapiro, *Adv. Chem. Phys.* 60 (1985) 371.
- [7] B. H. Lengsfeld and D. R. Yarkony, *Adv. Chem. Phys.* 82 (1992) 1.
- [8] M. Shapiro and R. Bersohn, *Annu. Rev. Phys. Chem.* 33 (1982) 409.
- [9] A. Brown and G. G. Balint-Kurti, *J. Chem. Phys.* 113 (2000) 1870.
- [10] T. P. Rakitzis, P. C. Samartzis, R. L. Toomes, T. N. Kitsopoulos, A. Brown, G. G. Balint-Kurti, O. S. Vasyutinskii, and J. A. Beswick, *Science* 300 (2003) 1936.
- [11] J. Zhang, C. W. Riehn, M. Dulligan, and C. Wittig, *J. Chem. Phys.* 104 (1996) 7027.
- [12] C. F. Bender and E. R. Davidson, *J. Chem. Phys.* 49 (1968) 4989.
- [13] T. H. Dunning and J. Chem. Phys. 65 (1976) 3854.
- [14] G. A. Segal and K. Wolf, *Chem. Phys.* 56 (1981) 321.
- [15] A. P. Hitchcock, G. R. J. Williams, C. E. Brion, and P. W. Langhoff, *Chem. Phys.* 88 (1984) 65.
- [16] S. C. Givertz and G. G. Balint-Kurti, *J. Chem. Soc., Faraday Trans. 2* 82 (1986) 1231.

- [17] M. H. Alexander, B. Pouilly, and T. Duhoo, *J. Chem. Phys.* 99 (1993) 1752.
- [18] I. H. Gersonde, S. Hennig, and H. Gabriel, *J. Chem. Phys.* 101 (1994) 9558.
- [19] T. Duhoo and B. Pouilly, *J. Chem. Phys.* 103 (1995) 182.
- [20] H. M. Lambert, P. J. Dagdigian, and M. H. Alexander, *J. Chem. Phys.* 108 (1998) 4460.
- [21] P. M. Regan, D. Ascenzi, A. Brown, G. G. Balint-Kurti, and A. J. Orr-Ewing, *J. Chem. Phys.* 112 (2000) 10259.
- [22] E. Tiemann, H. Kanamori, and E. Hirota, *J. Chem. Phys.* 88 (1988) 2457.
- [23] Y. Matsumi, K. Tonokura, M. Kawasaki, and T. Ibuki, *J. Chem. Phys.* 93 (1990) 7981.
- [24] J. Park, Y. Lee, and G. W. Flynn, *Chem. Phys. Lett.* 186 (1991) 441.
- [25] K. Tonokura, Y. Matsumi, M. Kawasaki, S. Tasaki, and R. Bersohn, *J. Chem. Phys.* 97 (1992) 8210.
- [26] D. Ascenzi, P. M. Regan, and A. J. Orr-Ewing, *Chem. Phys. Lett.* 310 (1999) 477.
- [27] P. M. Regan, S. R. Langford, D. Ascenzi, P. A. Cook, A. J. Orr-Ewing, and M. N. R. Ashfold, *Phys. Chem. Chem. Phys.* 1 (1999) 3247.
- [28] G. Peoux, M. Monnerville, T. Duhoo, and B. Pouilly, *J. Chem. Phys.* 107 (1997) 70.
- [29] B. Pouilly and M. Monnerville, *Chem. Phys.* 238 (1998) 437.
- [30] E. Martinez-Nunez and S. Vazquez, *Chem. Phys. Lett.* 425 (2006) 22.
- [31] A. G. Smolin, O. S. Vasyutinskii, G. G. Balint-Kurti, and A. Brown, *J. Phys. Chem. A* 110 (2006) 5371.
- [32] P. F. Zittel and D. D. Little, *J. Chem. Phys.* 71 (1979) 713.
- [33] F. Magnotta, D. J. Nesbitt, and S. R. Leone, *Chem. Phys. Lett.* 83 (1981) 21.
- [34] Z. Xu, B. Koplitz, and C. Wittig, *J. Chem. Phys.* 87 (1987) 1062.
- [35] Z. Xu, B. Koplitz, and C. Wittig, *J. Phys. Chem.* 92 (1988) 5518.
- [36] T. Kinugawa and T. Arikawa, *J. Chem. Phys.* 96 (1992) 4801.
- [37] R. Baumfalk, U. Buck, C. Frischkorn, N. H. Nahler, and L. Huwel, *J. Chem. Phys.* 111 (1999) 2595.
- [38] P. M. Regan, S. R. Langford, A. J. Orr-Ewing, and M. N. R. Ashfold, *J. Chem. Phys.* 110 (1999) 281.
- [39] T. P. Rakitzis, P. C. Samartzis, R. L. Toomes, and T. N. Kitsopoulos, *J. Chem. Phys.* 121 (2004) 7222.
- [40] I. Levy and M. Shapiro, *J. Chem. Phys.* 89 (1988) 2900.
- [41] C. Kalyanaraman and N. Sathyamurthy, *Chem. Phys. Lett.* 209 (1993) 52.
- [42] N. Chakrabarti and N. Sathyamurthy, *J. Phys. Chem. A* 102 (1998) 7089.
- [43] A. B. Alekseyev, H. P. Liebermann, D. B. Kokh, and R. J. Buenker, *J. Chem. Phys.* 113 (2000) 6174.
- [44] N. Balakrishnan, A. B. Alekseyev, and R. J. Buenker, *Chem. Phys. Lett.* 341 (2001) 594.
- [45] R. D. Clear, S. J. Riley, and K. R. Wilson, *J. Chem. Phys.* 63 (1975) 1340.
- [46] P. Brewer, P. Das, G. Ondrey, and R. Bersohn, *J. Chem. Phys.* 79 (1983) 720.
- [47] G. N. A. van Veen, K. A. Mohamed, T. Baller, and A. E. Devries, *Chem. Phys.* 80 (1983) 113.
- [48] D. J. Gendron and J. W. Hepburn, *J. Chem. Phys.* 109 (1998) 7205.
- [49] S. R. Langford, P. M. Regan, A. J. Orr-Ewing, and M. N. R. Ashfold, *Chem. Phys.* 231 (1998) 245.
- [50] P. M. Regan, D. Ascenzi, C. Clementi, M. N. R. Ashfold, and A. J. Orr-Ewing, *Chem. Phys. Lett.* 315 (1999) 187.
- [51] A. Brown and G. G. Balint-Kurti, *J. Chem. Phys.* 113 (2000) 1879.
- [52] G. G. Balint-Kurti, A. J. Orr-Ewing, J. A. Beswick, A. Brown, and O. S. Vasyutinskii, *J. Chem. Phys.* 116 (2002) 10760.

- [53] G. G. Balint-Kurti and A. Brown, Time-dependent wavepacket calculations for reactive scattering and photodissociation, in: *Theory of Chemical Reaction Dynamics*, eds. A. Lagana and G. Lendvay (Springer, Dordrecht, 2004) pp. 149.
- [54] K. A. Peterson, R. A. Kendall, and T. H. Dunning, *J. Chem. Phys.* 99 (1993) 1930.
- [55] A. A. Zavitsas, *J. Mol. Spectrosc.* 236 (2006) 168.
- [56] E. Safary, J. Romand, and B. Vodar, *J. Chem. Phys.* 19 (1951) 379.
- [57] J. B. Nee, M. Suto, and L. C. Lee, *J. Phys. B: At., Mol. Opt. Phys.* 18 (1985) L293.
- [58] F. Carnovale, R. Tseng, and C. E. Brion, *J. Phys. B: At., Mol. Opt. Phys.* 14 (1981) 4771.
- [59] J. N. Philippson, R. C. Shiell, E. Reinhold, and W. Ubachs, *J. Chem. Phys.* 129 (2008) 174310.
- [60] D. R. Yarkony, *Int. Rev. Phys. Chem.* 11 (1992) 195.
- [61] H. Lefebvre-Brion and R. Field, *Perturbations in the Spectra of Diatomic Molecules*, (Academic Press, Orlando, 1986).
- [62] R. N. Zare, *Angular Momentum* (John Wiley & Sons, Inc., New York, 1988).
- [63] E. J. Heller, *J. Chem. Phys.* 68 (1978) 2066.
- [64] E. J. Heller, *J. Chem. Phys.* 68 (1978) 3891.
- [65] E. J. Heller, *Acc. Chem. Res.* 14 (1981) 368.
- [66] G. G. Balint-Kurti, R. N. Dixon, and C. C. Marston, *Int. Rev. Phys. Chem.* 11 (1992) 317.
- [67] M. Y. Zhao, K. L. Han, C. Z. He, and J. Z. H. Zhang, *J. Theor. Comput. Chem.* 3 (2004) 443.
- [68] M. Y. Zhao, Q. T. Meng, T. X. Xie, K. L. Han, and G. Z. He, *Int. J. Quant. Chem.* 101 (2005) 153.
- [69] M. D. Feit, J. A. Fleck, Jr., and A. Steiger, *J. Comput. Phys.* 47 (1982) 412.
- [70] J. A. Fleck, J. R. Morris, and M. D. Feit, *Appl. Phys.* 10 (1976) 129.
- [71] T. S. Chu, Y. Zhang, and K. L. Han, *Int. Rev. Phys. Chem.* 25 (2006) 201.
- [72] T. S. Chu, R. F. Lu, K. L. Han, X. N. Tang, H. F. Xu, and C. Y. Ng, *J. Chem. Phys.* 122 (2005) 244322.
- [73] T. S. Chu, K. L. Han, and G. C. Schatz, *J. Phys. Chem. A* 111 (2007) 8286.
- [74] X. N. Tang, C. Houchins, K. C. Lau, C. Y. Ng, R. A. Dressler, Y. H. Chiu, T. S. Chu, and K. L. Han, *J. Chem. Phys.* 127 (2007) 164318.
- [75] T. S. Chu and K. L. Han, *Phys. Chem. Chem. Phys.* 10 (2008) 2431.
- [76] T. S. Chu, K. L. Han, M. Hankel, G. G. Balint-Kurti, A. Kuppermann, and R. Abrol, *J. Chem. Phys.* 130 (2009) 144301.
- [77] T. S. Chu, A. J. C. Varandas, and K. L. Han, *Chem. Phys. Lett.* 471 (2009) 222.
- [78] Y. Zhang, T. M. Xie, and K. L. Han, *J. Phys. Chem. A* 107 (2003) 10893.
- [79] Y. Zhang, T. X. Xie, K. L. Han, and J. Z. H. Zhang, *J. Chem. Phys.* 119 (2003) 12921.
- [80] Y. Zhang, T. X. Xie, K. L. Han, and J. Z. H. Zhang, *J. Chem. Phys.* 120 (2004) 6000.
- [81] Y. Zhang, T. X. Xie, K. L. Han, and J. Z. H. Zhang, *J. Chem. Phys.* 124 (2006) 134301.
- [82] R. F. Lu, T. S. Chu, and K. L. Han, *J. Phys. Chem. A* 109 (2005) 6683.
- [83] R. F. Lu, T. S. Chu, Y. Zhang, K. L. Han, A. J. C. Varandas, and J. Z. H. Zhang, *J. Chem. Phys.* 125 (2006) 133108.
- [84] R. F. Lu, P. Y. Zhang, T. S. Chu, T. X. Xie, and K. L. Han, *J. Chem. Phys.* 126 (2007) 124304.
- [85] J. C. Light, I. P. Hamilton, and J. V. Lill, *J. Chem. Phys.* 82 (1985) 1400.
- [86] O. Sharafeddin and J. Z. H. Zhang, *Chem. Phys. Lett.* 204 (1993) 190.
- [87] J. V. Lill, G. A. Parker, and J. C. Light, *Chem. Phys. Lett.* 89 (1982) 483.
- [88] D. H. Zhang and J. Z. H. Zhang, *J. Chem. Phys.* 101 (1994) 1146.
- [89] J. Z. H. Zhang, J. Q. Dai, and W. Zhu, *J. Phys. Chem. A* 101 (1997) 2746.
- [90] A. Vibok and G. G. Balint-Kurti, *J. Phys. Chem.* 96 (1992) 8712.
- [91] G. G. Balint-Kurti, R. N. Dixon, and C. C. Marston, *J. Chem. Soc., Faraday Trans.* 86 (1990)

1741.

- [92] C. E. Moore, Atomic Energy Levels, National Bureau of Standards National Standard Reference Data Series, Vol. 35 (U. S. GPO, Washington, D. C., 1971).
- [93] MOLPRO is a package of *ab initio* programs written by H. J. Werner, P. J. Knowles, R. D. Amos, A. Bernhardsson, A. Berning, P. Celani, D. L. Cooper, M. J. O. Deegan, A. J. Dobbyn, F. Eckert, *et al.* (University of Stuttgart, Germany / University of Birmingham, UK, 2002).
- [94] G. Parlant and D. R. Yarkony, J. Chem. Phys. 110 (1999) 363.
- [95] S. Lee, C. J. Williams, and K. F. Freed, Chem. Phys. Lett. 130 (1986) 271.
- [96] S. Lee and K. F. Freed, J. Chem. Phys. 87 (1987) 5772.
- [97] W. D. Zhou, Y. Yuan, and J. S. Zhang, J. Chem. Phys. 119 (2003) 9989.
- [98] R. Schinke, Photodissociation dynamics, in: Encyclopedia of Computational Chemistry, ed. P. von Ragué Schleyer (Wiley, New York, 1998).